Journal of Applied Mechanics and Technical Physics, Vol. 44, No. 1, pp. 90–101, 2003

NUMERICAL STUDY OF HYDRODYNAMICS AND HEAT AND MASS TRANSFER OF A DUCTED GAS–VAPOR–DROPLET FLOW

V. I. Terekhov and M. A. Pakhomov

UDC 536.24

A computational model has been developed to predict heat and mass transfer and hydrodynamic characteristics of a turbulent gas–vapor–droplet flow. Turbulent characteristics of the gas phase are computed using the k–ε model of turbulence. It is shown that, with increasing inlet droplet diameter, the rate of heat transfer between the duct surface and the vapor–gas mixture decreases appreciably, whereas the wall friction increases only insignificantly. The predicted values agree fairly well with available experimental and numerical data.

Key words: *two-phase flow, heat and mass transfer, turbulence, evaporation, gas–vapor–droplet system.*

Introduction. Gas–vapor–droplet flows have gained wide application in industry, for instance, in power-equipment components, in chemical apparatus, and in aircraft air-conditioning systems. With two-phase heat carriers, heat-transfer intensification is achieved at the expense of the latent evaporation heat absorbed during liquid-droplet evaporation in a two-component vapor–gas or in a single-component vapor flow. Involvement of a liquid phase and its boundary-layer evaporation necessitates taking into account the transfer of heat and mass between the phases. A detailed study of the mechanism underlying this transfer is especially important in the supercritical flow region of vapor generators, where the near-wall liquid film loses continuity and a transition from a dispersed-annular to dispersed flow mode occurs [1]. With an incondensable gas present in the mixture, one has to take into account the diffusion of vapor into the vapor–gas flow. The presence of a second gas-phase component (for instance, of air premixed to steam) substantially complicates the solution of the problem since it becomes necessary to simultaneously solve the energy and diffusion equations for the vapor–gas mixture.

Many works have been devoted to theoretical and experimental investigation of heat-transfer and hydrodynamic characteristics of two-phase turbulent flows [1–10]. Most extensively studied have been laminar and turbulent vapor–droplet flows [2–4]. Simultaneously, ducted turbulent gas–vapor–droplet flows, which are of considerable practical significance, have not been adequately considered (see, for instance, [5–10]).

The use of two-phase heat carriers in technical devices is seriously hampered by the lack of reliable experimental or numerical heat- and mass-transfer data for such flows and data on flow dynamics in them. Available numerical studies of heat-transfer features in gas–vapor–droplet flows [5, 7] use quite a number of simplifying assumptions lacking rigorous substantiation; among these assumptions, for instance, are the integral approach to predicting heat- and mass-transfer characteristics of two-phase flows [5] and the asymptotic theory of turbulent boundary layer [7].

Models based on solving systems of differential boundary-layer equations for a two-phase two-component mixture are devoid of the majority of the above deficiencies. Such models make it possible to more adequately predict heat- and mass-transfer processes in two-component gas–vapor–droplet flows [8–10]. The turbulent regime of a ducted two-phase gas–vapor–droplet flow was numerically examined in [8]. The computational model of [8] was constructed around the algebraic model of turbulence [11].

Kutateladze Institute of Thermal Physics, Siberian Division, Russian Academy of Sciences, Novosibirsk 630090. Translated from Prikladnaya Mekhanika i Tekhnicheskaya Fizika, Vol. 44, No. 1, pp. 108–122, January–February, 2003. Original article submitted May 14, 2002; revision submitted August 26, 2002.

 0021-8944/03/4401-0090 $25.00

On the whole, the problem statement in the present study is much the same as in [8], but the two-parametric k–ε-model of turbulence is used to close the governing equations [12]. Impact of many factors, including deposition of droplets onto the duct wall and their evaporation on the duct surface and in the duct volume, is examined. Results of testing the model are reported and compared with available experimental data.

1. Physical Model. We consider heat- and mass-transfer and hydrodynamic characteristics of a ducted turbulent gas–vapor–droplet flow with allowance for droplet evaporation, interaction between the phases, droplet deposition onto the duct wall, droplet-to-wall heat transfer, and vapor diffusion into the vapor–gas mixture. We imply that the annular near-wall liquid film has already dried out (i.e., the wall temperature $T_{\rm w}$ is higher than the Leidenfrost temperature for the droplets) [1]. Radiative heat transfer is ignored [3–10]. All droplets are assumed to undergo instantaneous evaporation as they touch the wall, and the duct wall, therefore, always remains dry. Conductive heat transfer due to immediate droplet-wall contacts is treated within the framework of the model [5]. In the present work, a three-stage mechanism of heat transfer in the two-phase flow is considered:

1) the wall heat is transferred to droplets on the duct surface to be subsequently spent on their evaporation;

2) the wall heat is transferred to the vapor–gas mixture;

3) some part of the heat transferred to the vapor–gas mixture is subsequently transferred to liquid droplets and is spent on their heating and evaporation.

The volume fraction of the liquid phase is small ($Z_{\rm liq} < 10^{-4}$), and the droplets are rather fine (diameter $d_1 < 100$ μm). We assume that all particles in each cross-section of the duct have identical sizes and are uniformly distributed over the volume. This mechanism can be realized in practice due to intense turbulent mixing of the flow and droplets across the duct. No coalescence or fractionation of droplets occurs in the flow [5]. According to [1], this assumption can be adopted provided that $Z_{\rm liq} \leqslant 10^{-4}$.

In the vapor–gas flow, the droplets act as a distributed sink of heat and a distributed source of vapor. The mixture gives off heat to liquid droplets, and the released vapor undergoes heating to the main-flow temperature and diffuses into regions with a lower vapor content. The heat transfer from the vapor–gas mixture to the droplets is due to heat conduction and convection. The droplets and their evaporation exert no influence on turbulent characteristics of the gas phase.

In the inlet plane of the duct, the distributions of temperatures and velocities of the phases are uniform. All droplets at the duct inlet have identical sizes and temperatures. In the computations, the initial temperatures of the phases could be assumed to be either identical or different.

2. Mathematical Model. Under the adopted assumptions, the hydrodynamic and heat- and mass-transfer characteristics of the two-phase flow can be described by a system of differential axisymmetric-flow equations.

System of Governing Equations. The continuity equation, the equation of motion, the energy equation, and the mass-transfer equation for the binary vapor–gas mixture in the boundary-layer approximation are

$$\frac{\partial U}{\partial x} + \frac{1}{r}\,\frac{\partial (rV)}{\partial r} = \frac{Jn\pi d^2}{\rho},$$

$$\rho\Big(U\,\frac{\partial U}{\partial x} + V\,\frac{\partial U}{\partial r}\Big) = -\frac{\partial P}{\partial x} + \frac{\rho}{r}\,\frac{\partial}{\partial r}\Big(r(\mu+\mu_{\rm t})\,\frac{\partial U}{\partial r}\Big) - C_D n\rho(U-U_{\rm liq})|U-U_{\rm liq}|A_{\rm liq},$$

$$\rho C_p\Big(U\,\frac{\partial T}{\partial x} + V\,\frac{\partial T}{\partial r}\Big) = \frac{1}{r}\,\frac{\partial}{\partial r}\Big[r\Big(\frac{\mu}{\rm Pr} + \frac{\mu_{\rm t}}{{\rm Pr}_{\rm t}}\Big)\frac{\partial T}{\partial r}\Big] - \alpha n\pi d^2(T-T_{\rm liq}) + \rho D_{\rm t}\,\frac{\partial K_{\rm vap}}{\partial r}\,(C_{p,{\rm vap}} - C_{p,{\rm air}})\frac{\partial T}{\partial r}, \qquad (1)$$

$$\rho\Big(U\,\frac{\partial K_{\rm vap}}{\partial x} + V\,\frac{\partial K_{\rm vap}}{\partial r}\Big) = \frac{\rho}{r}\,\frac{\partial}{\partial r}\Big[r\Big(\frac{\mu}{\rm Sc} + \frac{\mu_{\rm t}}{{\rm Sc}_{\rm t}}\Big)\frac{\partial K_{\rm vap}}{\partial r}\Big] + Jn\pi d^2,$$

$$\rho = (1-Z_{\rm liq})P/(RT).$$

Here U and V are the axial and radial velocities, x and r are the axial and radial coordinates, J is the vapor-mass flux from the surface of an evaporating droplet, $n = \rho M_{{\rm liq},1}/(\rho_{\rm liq}\pi d_1^3/6)$ is the numerical concentration of particles in unit volume, ρ is the density, μ is the dynamic viscosity, C_p is the specific heat capacity, P is the pressure, $A_{\rm liq} = \pi d^2/4$ is the cross-sectional area of a particle, T is temperature, α is the coefficient of heat transfer to an evaporating droplet, D is the vapor diffusivity in the vapor–gas mixture, $K_{\rm vap}$ is the mass concentration of vapor in the binary vapor–gas mixture, and ${\rm Pr} = C_p\mu/\lambda$ and ${\rm Sc} = \nu/D$ are the Prandtl and Schmidt numbers, respectively. The subscripts "air," "liq," and "vap" refer to air, droplet, and vapor, respectively; the subscript "t" marks turbulent characteristics.

To determine the turbulent viscosity of the gas phase, we used the k–ε model of turbulence proposed in [12]. This modification of the k–ε model was chosen considering the fact that this modification, as compared to other models, more adequately predicts characteristics of carrier-phase turbulence [13, 14]. The transfer equations for turbulent kinetic energy and for the rate of its dissipation are

$$\rho\Big(U\,\frac{\partial k}{\partial x}+V\,\frac{\partial k}{\partial r}\Big)=\frac{\rho}{r}\,\frac{\partial}{\partial r}\Big[r\Big(\mu+\frac{\mu_{\rm t}}{\sigma_k}\Big)\frac{\partial k}{\partial r}\Big]+G_k-\rho\varepsilon,$$

$$\rho\Big(U\,\frac{\partial \varepsilon}{\partial x}+V\,\frac{\partial \varepsilon}{\partial r}\Big)=\frac{\rho}{r}\,\frac{\partial}{\partial r}\Big[r\Big(\mu+\frac{\mu_{\rm t}}{\sigma_\varepsilon}\Big)\frac{\partial \varepsilon}{\partial r}\Big]+\frac{C_{\varepsilon1}\varepsilon f_1 G_k}{k}-\frac{C_{\varepsilon2}\varepsilon^2\rho f_2}{k},$$

where k is the turbulent kinetic energy, ε is the rate of its dissipation, $\mu_{\rm t}=C_\mu f_\mu\rho k^2/\varepsilon$, $\sigma_k=1.4$, $\sigma_\varepsilon=1.3$, $C_\mu=0.09$, $C_{\varepsilon1}=1.45$, $C_{\varepsilon2}=1.9$, $f_1=1$, $G_k=\mu_{\rm t}(\partial U/\partial r)^2$, $f_2=[1-\exp(-y_+/6)]^2[1-0.3\exp(-({\rm Re}_{\rm t}^{3/4}/6.5)^2)]$, $f_\mu=[1-\exp(-y_+/26)]^2(1+4.1/{\rm Re}_{\rm t}^{3/4})$, and ${\rm Re}_{\rm t}=k^2/(\varepsilon\nu)$.

The expression for the derivative $\partial P/\partial x$ in the equation of motion over the inlet section of the duct can be represented in the form

$$-\frac{\partial P}{\partial x}=\rho U_0\,\frac{\partial U_0}{\partial x}. \tag{2}$$

In formula (2), the term taking into account the effect due to the droplets is omitted. Estimates show that, in the range of droplet concentrations dealt with in the present study and at small values of the relative velocity between the phases, the computation results obtained with and without this term differ only within 5%.

To determine the derivative $\partial P/\partial x$, we use the equation of constancy of the mass-flow rate in the duct

$$\rho U_0\pi(R-\delta)^2+2\rho\pi\int\limits_{R-\delta}^{R}Ur\,dr=G_1+G_2, \tag{3}$$

where R is the duct radius, δ is the boundary-layer thickness, U_0 is the flow velocity at the duct axis, and G_1 and G_2 are the mass-flow rate of the mixture in the current cross-section and the rate of the mass flow due to vaporization, respectively. The formulas for G_1 and G_2 in (3) have the form

$$G_1=\rho U_{\rm m}\pi R^2(M_{\rm air}+M_{\rm vap}),\qquad G_2=\rho_{\rm vap}U_{\rm m}\pi R^2(M_{{\rm vap},i}-M_{{\rm vap},i-1}).$$

Finally, the equation for the axial velocity U_0 transforms into

$$U_0=\frac{1}{\rho\pi(R-\delta)^2}\Big(G_1+G_2-2\rho\pi\int\limits_{R-\delta}^{R}Ur\,dr\Big). \tag{4}$$

Balance Equations for Vapor Energy and Mass at the Surface of an Evaporating Droplet. We supplement relations (1) with the energy-balance equation for the liquid phase

$$C_{p,{\rm liq}}\rho_{\rm liq}\,\frac{\pi d^3}{6}\,\frac{\partial T_{\rm liq}}{\partial t}=\alpha\pi d^2(T-T_{\rm liq})-J\pi d^2[L+C_{p,{\rm vap}}(T-T_{\rm liq})] \tag{5}$$

and with the equation of vapor-mass conservation on the surface of an evaporating droplet [15]

$$J=JK^*_{\rm vap}-\rho_{\rm vap}D\,\frac{\partial K^*_{\rm vap}}{\partial r}, \tag{6}$$

where L is the specific phase-transition heat and $K^*_{\rm vap}$ is the vapor concentration at the droplet surface under saturation conditions for the droplet temperature $T_{\rm liq}$. Taking into account that the diffusional Stanton number ${\rm St_d}$ has the form

$${\rm St_d}=-\frac{\rho_{\rm vap}D}{\rho U(K^*_{\rm vap}-K_{\rm vap})}\,\frac{\partial K^*_{\rm vap}}{\partial r},$$

we can write the equation of mass conservation (6) as

$$J={\rm St_d}\rho U b_{1,{\rm d}}, \tag{7}$$

where

$$b_{1,{\rm d}}=(K^*_{\rm vap}-K_{\rm vap})/(1-K^*_{\rm vap}) \tag{8}$$

is the diffusional injection parameter determined from the saturation curve.

The equations for the heat and mass fluxes from the surface of a non-evaporating sphere are [1]

$$\mathrm{Nu_p} = \alpha_\mathrm{p} d/\lambda = 2 + 0.6\,\mathrm{Re_{liq}^{1/2}}\,\mathrm{Pr^{1/3}}, \qquad \mathrm{Sh_p} = \beta d/D = 2 + 0.6\,\mathrm{Re_{liq}^{1/2}}\,\mathrm{Sc^{1/3}}.$$

Here $\mathrm{Re_{liq}} = \rho d\sqrt{(U-U_\mathrm{liq})^2 + (V-V_\mathrm{liq})^2}/\mu$ is the particle Reynolds number based on the slip velocity of the phases, $\mathrm{Sh_p}$ is the Sherwood number, and β is the mass-transfer coefficient; the subscript "p" refers to non-evaporating particles.

The diffusional Stanton number can be expressed as [15]

$$\mathrm{St_d} = \mathrm{Sh_p}/(\mathrm{Re_{liq}}\,\mathrm{Sc}).$$

Then, Eq. (6) transforms into

$$J = (2 + 0.6\,\mathrm{Re_{liq}^{1/2}}\,\mathrm{Sc^{1/3}})\rho U b_{1,\mathrm{d}}/(\mathrm{Re_{liq}}\,\mathrm{Sc}). \tag{9}$$

According to [16], the coefficient of heat transfer to evaporating droplets α can be related to the heat-transfer coefficient of non-evaporating droplets α_p by the following formula:

$$\alpha = \alpha_\mathrm{p}/[1 + C_p(T - T_\mathrm{liq})/L]. \tag{10}$$

The material-balance equation for a binary vapor–air mixture is

$$K_\mathrm{air} + K_\mathrm{vap} = 1.$$

For a ternary vapor–gas–liquid mixture, the analogous equation is

$$M_\mathrm{air} + M_\mathrm{vap} + M_\mathrm{liq} = 1. \tag{11}$$

The relation between the mass concentrations of the mixture components (K and M) is given by the formulas

$$K_\mathrm{vap} = M_\mathrm{vap}/(M_\mathrm{air} + M_\mathrm{vap}), \qquad K_\mathrm{air} = M_\mathrm{air}/(M_\mathrm{air} + M_\mathrm{vap}) = 1 - K_\mathrm{vap}. \tag{12}$$

The current droplet diameter in the ith section can be found using the formula [8]

$$\rho_\mathrm{liq}\pi d_i^3/6 = \rho_\mathrm{liq}\pi d_{i-1}^3/6 - J\pi d_{i-1}^2 \Delta x/U_{\mathrm{m},i},$$

where Δx is the distance between the computation cross-sections along the axial coordinate and $U_{\mathrm{m},i}$ is the mean flow velocity in the current cross-section. The choice of the velocity $U_{\mathrm{m},i}$ as a characteristic mean velocity of the flow was motivated by radial uniformity of droplet sizes.

In flows with intense evaporation, the gas-phase flow rate increases in the downstream direction due to vapor generation. The mean-mass velocity of the vapor–gas mixture in the current cross-section of the duct, with allowance for the vapor-mass income from evaporating droplets, was calculated from the formula

$$U_{\mathrm{m},i} = U_{\mathrm{m},i-1}/[1 - n\rho_\mathrm{liq}(d_i^3 - d_{i-1}^3)/\rho].$$

The turbulent Prandtl and Schmidt numbers were assumed to be uniform both over the duct length and over the duct radius: $\mathrm{Pr_t} = \mathrm{Sc_t} = 0.9$.

A Model for Droplet Deposition onto the Duct Wall from the Two-Phase Flow. To predict the rate of deposition of liquid droplets onto the duct wall from the turbulent flow, we use the theoretical dependence proposed by Gusev et al. [17]:

$$k_{\mathrm{liq}+} = \frac{k_\mathrm{liq}}{Z_\mathrm{liq} U_*} = \frac{0.115/(B^{0.75}\tau_+^{3/8}) + 2.5\cdot 10^{-4}\tau_+^{2.5}}{1 + 10^{-3}\tau_+^{2.5} + 1.25\cdot 10^{-3}\tau_+^3/\sqrt{R_+}}. \tag{13}$$

Here k_liq is the rate of droplet deposition onto the wall, $B = 12.73\sqrt{\rho/\rho_\mathrm{liq}}\pi\nu^3/(1.381\cdot 10^{-23} T U_*)$ is the factor taking into account the influence of Brownian diffusion on droplet deposition [17], $\tau_+ = \rho\tau U_*^2/\mu$ is the dimensionless relaxation time of the droplets, $\tau = \rho_\mathrm{liq} d^2/(18\mu(1 + \mathrm{Re_{liq}^{2/3}}/6))$ is the relaxation time of the droplets, $E = 1 + \mathrm{Re_{liq}^{2/3}}/6$ is the correction factor that makes allowance for the deviation of the flow around a droplet from the Stokes law, U_* is the dynamic velocity, $R_+ = RU_*/\nu$ is the dimensionless duct radius, and R is the duct radius. The subscript "plus" indicates that the parameter is expressed in terms of dynamic variables.

To determine the mass concentration of particles deposited on the duct wall ($M_{\text{liq,w}}$), we use the following algebraic relations:

$$M_{\text{liq,w}} = \frac{n_{\text{w}}\rho_{\text{liq}}\pi d^3}{6\rho}, \quad n_{\text{w}} = \frac{N_{\text{w}}}{\pi R^2 \Delta x}, \quad N_{\text{w}} = \frac{6m_{\text{w}}}{\rho_{\text{liq}}\pi d^3}, \quad m_{\text{w}} = J_{\text{w}}\,\Delta x\, 2\pi\,\Delta r\,\Delta t.$$

Here $J_{\text{w}} = k_{\text{liq}}\rho_{\text{liq}}$ is the mass velocity of droplet deposition, Δx and Δr are the steps along the axial and radial coordinates, Δt is time, m_{w} is the mass of the liquid on the duct wall, N_{w} is the number of droplets deposited onto the wall, n_{w} is the numerical concentration of the liquid phase deposited on the wall from the two-phase flow, and $n = n_{i-1} - n_{\text{w}}$ is the current numerical concentration of particles in the flow.

Conductive Droplet-to-Wall Heat Transfer. During deposition of droplets onto the wall, some portion of the wall heat flux is spent on their evaporation. As in the majority of previous models (see, for instance, [5]), we assume that the heat fluxes obey the superposition principle. The heat flux supplied to the duct surface, q_{w}, includes components corresponding to the wall-to-droplet heat flux ($q_{\text{w,liq}}$) and to the wall-to-mixture heat flux ($q_{\text{w,fl}}$).

According to [5], the density of the wall-to-droplet heat flux can be written as

$$q_{\text{w,liq}} = \chi J_{\text{w}} L M_{\text{liq,m}}, \tag{14}$$

where χ is the droplet-to-wall heat-transfer efficiency and $M_{\text{liq,m}}$ is the mean-mass concentration of droplets in a duct cross-section, defined as

$$M_{\text{liq,m}} = \frac{2}{U_{\text{m}}R^2}\int\limits_0^R M_{\text{liq}} U r\, dr.$$

For $T_{\text{w}} > T_{\text{liq}}$, the droplet-to-wall heat-transfer efficiency is given by the formula $\chi = \exp\left[1 - (T_{\text{w}}/T_{\text{liq}})^2\right]$ recommended in [5].

Equation of Particle Motion. All computations in the present study were performed for a vertically oriented duct. The following forces acting on the particles were taken into account: the drag force, the gravity force, and the buoyancy force. The Saffman and Magnus forces were ignored. The aerodynamic forces due to the pressure gradient, attached mass, and Basset effect were assumed to be negligible since they are proportional to the gas/liquid density ratio, which, in the majority of practical cases, is of the order of 10^{-3}.

The equation of droplet motion with allowance for the aerodynamic drag, gravity, and buoyancy forces can be written in the following vector form:

$$m_{\text{liq}}\frac{d\boldsymbol{U}_{\text{liq}}}{dt} = C_D\rho(\boldsymbol{U} - \boldsymbol{U}_{\text{liq}})\,|\boldsymbol{U} - \boldsymbol{U}_{\text{liq}}|A_{\text{liq}} + m_{\text{liq}}\boldsymbol{g}\Big(1 - \frac{\rho}{\rho_{\text{liq}}}\Big). \tag{15}$$

Here $m_{\text{liq}} = \rho_{\text{liq}}\pi d^3/6$ is the mass of a droplet, C_D is its drag coefficient, t is time, and $\boldsymbol{g}$ is the free-fall acceleration.

The projections of this equation onto the x and r axes have the form

$$m_{\text{liq}}\frac{dU_{\text{liq}}}{dt} = C_D\rho(U - U_{\text{liq}})\,|\boldsymbol{U} - \boldsymbol{U}_{\text{liq}}|A_{\text{liq}} \pm m_{\text{liq}}g\Big(1 - \frac{\rho}{\rho_{\text{liq}}}\Big)$$

in the axial direction x or

$$m_{\text{liq}}\frac{dV_{\text{liq}}}{dt} = C_D\rho(V - V_{\text{liq}})\,|\boldsymbol{V} - \boldsymbol{V}_{\text{liq}}|A_{\text{liq}}$$

in the radial direction r.

For evaporating droplets, the drag coefficient C_D is given by the expression [5]

$$C_D = C_{D,\text{p}}/[1 + C_p(T - T_{\text{liq}})/L],$$

where $C_{D,\text{p}}$ is the friction coefficient, given, for non-evaporating droplets, by the formulas

$$C_{D,\text{p}} = \begin{cases} 24/\,\text{Re}_{\text{p}}, & \text{Re}_{\text{p}} \leqslant 1, \\ 24(1 + \text{Re}_{\text{p}}^{2/3}/6)/\text{Re}_{\text{p}}, & \text{Re}_{\text{p}} > 1. \end{cases}$$

Determination of Fluctuating Intensities of the Gas and Dispersed Phases. In the computations, all particles were assumed to be sufficiently large, so that the relaxation time of each particle τ was longer than the integral

time scale of turbulence Ω. The value of Ω, needed for determination of the radial fluctuating velocity of the gas phase, is given by the formula [18]

$$\Omega_+ = \rho\Omega U_*^2/\mu = \sqrt{l_{0+}^2 + l_+^2},$$

which, as $y_+ \to 0$, reduces to the relation $\Omega_+ = l_{0+} \approx 10$ (in the viscous sublayer, the integral time scale of turbulence is assumed to be constant), whereas in the core of the turbulent flow, it reduces to the relation $\Omega_+ = l_+ = \rho l U_*/\mu$, where l_+ is the relative mixing-path length and l is the mixing-path length given by the Prandtl–Nikuradze formula [18]

$$l = R[0.14 - 0.08(r/R)^2 + 0.06(r/R)^4].$$

The radial component of the root-mean-square fluctuations of the gas-phase velocity can be found from the relation [19]

$$\langle v^2 \rangle = \mu_\mathrm{t}/(\rho\Omega \mathrm{Sc}_\mathrm{t}). \tag{16}$$

The root-mean-square fluctuating velocity of the carrier phase in the axial direction is [19]

$$\langle u^2 \rangle \approx 1.3k. \tag{17}$$

For relatively large droplets, the turbulence intensity of the dispersed phase is given by the relations [19]

$$\langle v_\mathrm{liq}^2 \rangle = \langle v^2 \rangle \Omega/\tau, \quad \Omega = L_\mathrm{e}/\sqrt{\langle v^2 \rangle}, \quad L_\mathrm{e} = 0.14R, \tag{18}$$

where L_e is the carrier-phase turbulence scale.

Boundary and Inlet Conditions. We have

$$\frac{\partial T}{\partial r} = \frac{\partial K_\mathrm{vap}}{\partial r} = \frac{\partial U}{\partial r} = \frac{\partial k}{\partial r} = \frac{\partial \varepsilon}{\partial r} = V = 0 \tag{19}$$

at the duct axis ($r = 0$),

$$-\lambda \frac{\partial T}{\partial r} = q_\mathrm{w,fl}, \quad \frac{\partial K_\mathrm{vap}}{\partial r} = \frac{\partial k}{\partial r} = U = V = k = 0, \quad \varepsilon_\mathrm{w} = \nu \Big(\frac{\partial^2 k}{\partial r^2} \Big)_\mathrm{w} \tag{20}$$

at the wall ($r = R$), and

$$\begin{gathered} U = U_1, \quad V = V_1, \quad T = T_1, \quad M_\mathrm{liq} = M_\mathrm{liq,1}, \quad T_\mathrm{liq} = T_\mathrm{liq,1}, \\ d = d_1, \quad K_\mathrm{vap} = K_{V1}, \quad k = k_1, \quad \varepsilon = \varepsilon_1 \end{gathered} \tag{21}$$

in the inlet cross-section of the duct.

In this study, we assume that the level of turbulence of the gas phase at the duct inlet is $\mathrm{Tu} = \sqrt{(1/3)(\langle u^2 \rangle + \langle v^2 \rangle + \langle w^2 \rangle)}/U = 3\%$.

Relations (1)–(18) with the appropriate boundary and initial conditions (19)–(21) represent a closed system of equations for heat- and mass-transfer processes in a turbulent two-phase flow. This system allows one to calculate all quantities of interest (distributions of temperatures and concentrations of the phases and components of the vapor–gas mixture) and predict the downstream evolution of particle sizes.

3. Numerical Implementation and Testing of the Model. The partial differential equations were numerically solved with the help of the Crank–Nicholson finite-difference scheme [20], by transforming the initial differential equations to a system of discrete linear algebraic equations. The resultant tridiagonal system of equations was solved by the sweep method according to the Thomas algorithm, described in more detail elsewhere [20]. We used a computational grid with a variable mesh size, decreasing toward the duct wall. In the axial direction, the grid was uniform.

All computations were performed on a grid with 201 nodal points in the axial direction and 101 nodal points in the radial direction. In addition, some methodical computations were performed on a finer, 201×201 computational grid. These computations showed that the difference between the computed carrier-flow temperature and droplet-diameter profiles in the two cases was well within 0.5%. In further computations, to examine heat and mass transfer in the turbulent gas–vapor–droplet flow, we routinely used the 201×101 computation grid.

To test the adopted model of turbulence, we compared the data yielded by this model with direct-simulation data and experimental results obtained in [21] for an isothermal single-phase ducted airflow and also with the

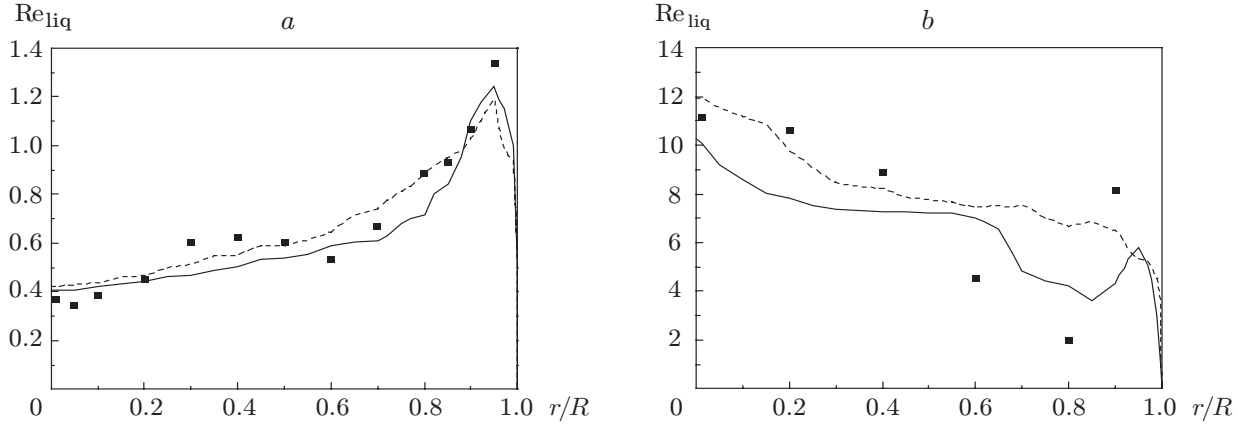

Fig. 1. Radial distributions of measured and calculated Reynolds numbers of glass particles in the steady-state ducted flow: (a) downward flow; (b) upward flow; the solid and dashed curves refer to the model of [12] and the algebraic model of [11]; the points show the experimental data of [23] (a) and [24] (b).

experimental data of [22]. The data yielded by the k–ε model of turbulence were found to fairly well predict heat-transfer features for a turbulent single-phase gas flow [15].

To compare simulation data for two-phase flows with previously reported experimental results, we used the experimental data of [23] for a downward gas–glass particle flow and the data of [24] for an upward gas–glass particle flow. The predicted and measured radial distributions of the particle Reynolds number are shown in Fig. 1. The input data for the computations were chosen to reproduce the experimental conditions of [23] ($2R = 46$ mm, Re = 12,300, $U_0 = 4$ m/sec, $M_\mathrm{p} = 2\%$, $d = 50$ μm, $\rho_\mathrm{p} = 2550$ kg/m^3, $U_* = 0.24$ m/sec, and $\tau_+ = 79$) and [24] ($2R = 12.7$ mm, Re = 24,500, $U_0 = 28.7$ m/sec, $M_\mathrm{p} = 26\%$, $d = 62$ μm, $\rho_\mathrm{p} = 2640$ kg/m^3, $U_* = 1.61$ m/sec, and $\tau_+ = 5417$). To perform the computations, either the algebraic model of turbulence [11] or the k–ε model of turbulence [12] was used.

The data obtained for the two-phase flow of the mixture with a low concentration of the dispersed phase show that both models of turbulence rather adequately reproduce the measured radial distributions of the particle Reynolds number (Fig. 1a). The computed data, as well as the experimental results, show that the slip velocity of the phases increases in the near-wall zone of the downward flow.

For the upward flow of the gas suspension (Fig. 1b), the distribution of the slip velocity changes for the opposite one: the maximum velocity is attained at the duct axis and the minimum one near the duct wall. It is hardly possible to conclude definitely from Fig. 1b which of the two models more adequately predicts the behavior of the particle Reynolds number Re_liq in the flow with a high concentration of the dispersed phase. In the latter case, effects of particle collisions with each other and with the duct wall are manifested. This might be the reason for the observed difference between the predicted and measured values. In a flow with a high mass concentration of the dispersed phase, effects due to inter-particle and particle-wall collisions, and also due to possible rotation of the dispersed phase, could exert a substantial influence on the flow pattern [25]. Nonetheless, satisfactory agreement between the predictions of the two models for the near-axis region of the flow and the experimental results is worth noting. The model of [12], unlike the model of [11], predicts an increase in Re_liq in the near-wall zone.

It should be noted that both models, [11] and [12], as applied to upward or downward flows, yield results being in good qualitative agreement with the data of [26] obtained for a vertical isothermal dispersed flow in a cylindrical duct.

Figure 2 compares the radial distributions of relative axial- and radial-velocity fluctuations of the gas and dispersed phases with the experimental data of [27]. The experimental data in [27] were obtained for a downward flow of an air–glass particle mixture by means of laser-Doppler anemometry. The input data for the computations were chosen to comply with the experimental conditions adopted in [27]: $2R = 46$ mm, $U_0 = 5.2$ m/sec, $d = 50$ μm, $\rho_\mathrm{p} = 2550$ kg/m^3, $U_* = 0.31$ m/sec, $M_\mathrm{p} = 5\%$, $\tau_+ = 125$, and Re = 15,300.

The computed intensities of the axial- and radial-velocity fluctuations of the gas phase compare well with the experimental data. The agreement between the experimental data and the values predicted by the theoretical model of [19] is somewhat worse. The distributions plotted in Fig. 2 show that the intensity of radial fluctuations

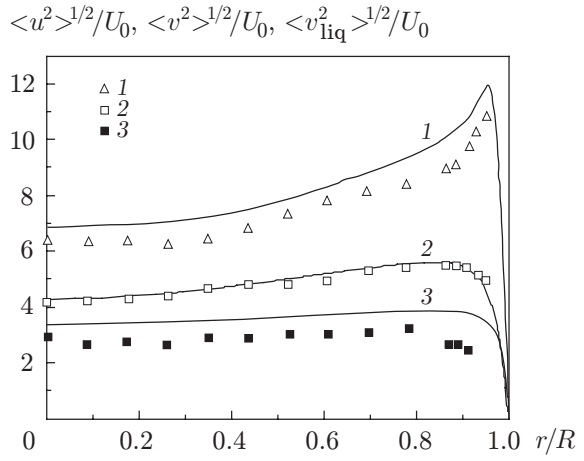

Fig. 2

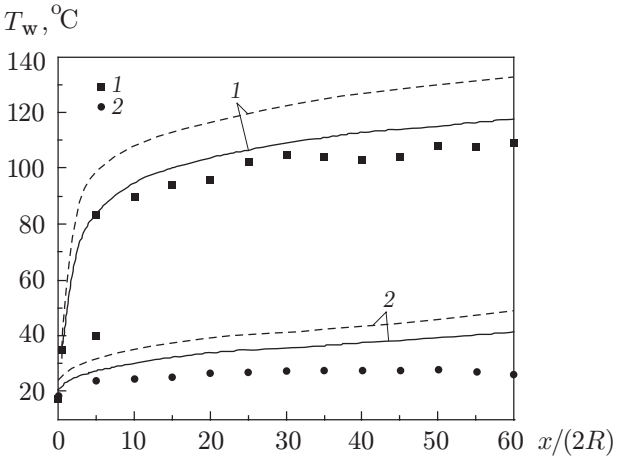

Fig. 3

Fig. 2. Distribution of the root-mean-squared velocity fluctuations of the air–glass particle flow: the curves refer to the calculated data and the symbols are the experimental data of [27] for $\langle u^2\rangle^{1/2}/U_0$ (1), $\langle v^2\rangle^{1/2}/U_0$ (2), and $\langle v_{\rm liq}^2\rangle^{1/2}/U_0$ (3).

Fig. 3. Variation of wall temperature along the duct in a single-component vapor–droplet flow for $M_{\rm liq,1} = 0.35$, $q_{\rm w} = 7.14$ kW/m^2 (1), and $M_{\rm liq,1} = 0.43$, $q_{\rm w} = 2.13$ kW/m^2 (2): the solid and dashed curves refer to the models of [12] and [11], respectively; the points show the experimental data of [3].

of particle velocity is lower than the corresponding value for the carrier phase. This fact can be explained as follows. The Stokes number of the large-eddy motion is defined as $\mathrm{S} = \tau/\Omega$. For the conditions under consideration, $\mathrm{S} \approx 1$, i.e., the particles readily get involved into the large-eddy motion and take off energy from turbulent carrier-phase eddies. A decrease in the intensity of the radial-velocity fluctuations of the gas phase causes a decrease in the particle-velocity fluctuations [27].

To estimate the accuracy in predicting the heat-transfer characteristics of a vapor–droplet flow, we compared the results yielded by the present computational model with the experimental data of [3]. The wall-temperature profile over the duct length for the vapor–droplet flow is shown in Fig. 3. The input data for the computations were as follows: $2R = 10$ mm, saturation pressure $P_{\rm sat,1} = 3.08 \cdot 10^5$ Pa, $T_{\rm sat,1} = T_{\rm liq,1} = T_1 = 300$ K, $d_1 = 30$ μm, and inlet Reynolds number $\mathrm{Re}_1 = 5.1 \cdot 10^5$. The working liquid was Freon R-113. It follows from Fig. 3 that the predicted and measured data agree with each other under high thermal loads better than at low values of $q_{\rm w}$. A possible reason for the observed difference between the predicted and measured data is inconsistency between the adopted and actual mechanisms of heat transfer between the gas–droplet flow and the wall. In particular, as the wall temperature decreases, the formation of liquid films on the wall surface, ignored in the present model, becomes more probable. At the same time, the k–ε model provides better agreement with the experimental data, compared to the algebraic model of [11].

An analysis of the data in Figs. 1–3 allows us to conclude that the k–ε model of turbulence and the algebraic relations for the root-mean-square fluctuations of gas-phase and particle velocities rather adequately predict fluctuating processes, dynamics of both phases, and heat- and mass-transfer features in developed two-phase flows.

4. Computation Data. The computations were performed for an air–steam flow with water droplets (under atmospheric pressure). The duct length was 2 m, the inner duct diameter was 0.02 m, the inlet temperature of the vapor–gas flow $T_1 = 293$–373 K, the flow Reynolds number $\mathrm{Re} = 5 \cdot 10^3$–$10^6$, the inlet droplet diameter $d_1 = 0.1$–100 μm, the dimensionless relaxation time of the droplets $\tau_+ = 10^{-3}$–10^3, the mass fraction of the droplet phase $M_{\rm liq,1} = 0$–0.1, and the mass fraction of air $M_{\rm air,1} = 0$–0.8. All computations were performed for a fixed wall heat-flux density ($q_{\rm w} = \mathrm{const}$), namely, for $q_{\rm w} = 1$ kW/m^2.

Figure 4 illustrates how the mass concentration of liquid droplets affects the surface friction and the rate of heat transfer ($C_{\rm fr,vap}$ and $\mathrm{Nu}_{\rm vap}$ are the friction and heat-transfer coefficients of a single-phase vapor flow). An increase in the liquid-phase concentration and initial particle size causes an increase in the friction coefficient

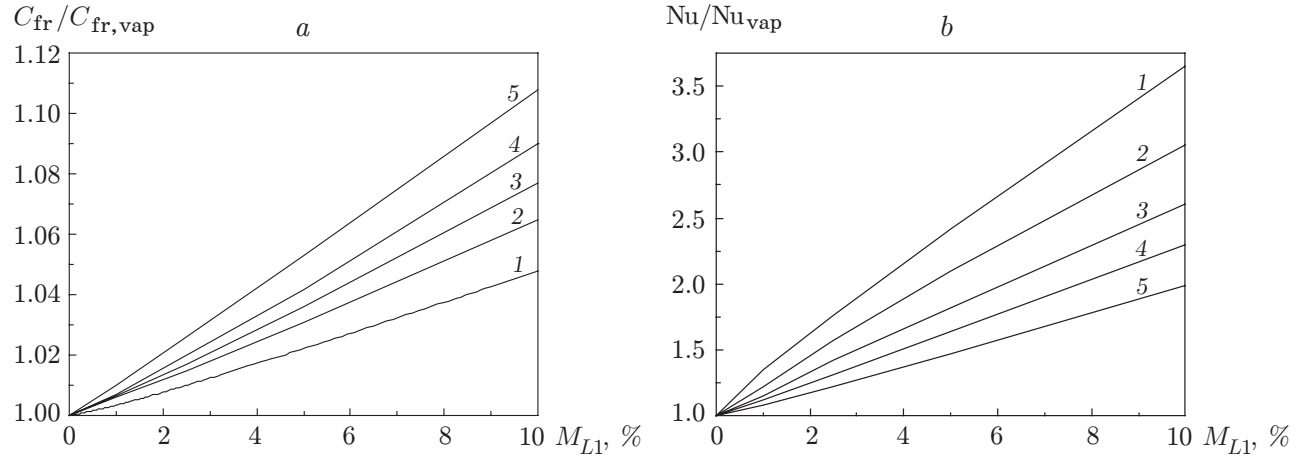

Fig. 4. Variation of the relative friction coefficient (a) and heat-transfer intensification ratio $\mathrm{Nu}/\mathrm{Nu}_{\rm vap}$ (b) in the gas–vapor–droplet flow with $\mathrm{Re} = 13{,}000$, $x/(2R) = 20$: $d = 1$ μm, $\tau_+ = 0.1$ (1), and $d = 10$ μm and $\tau_+ = 8$ (2), $d = 30$ μm and $\tau_+ = 70$ (3), $d = 50$ μm and $\tau_+ = 190$ (4), and $d = 100$ μm and $\tau_+ = 760$ (5).

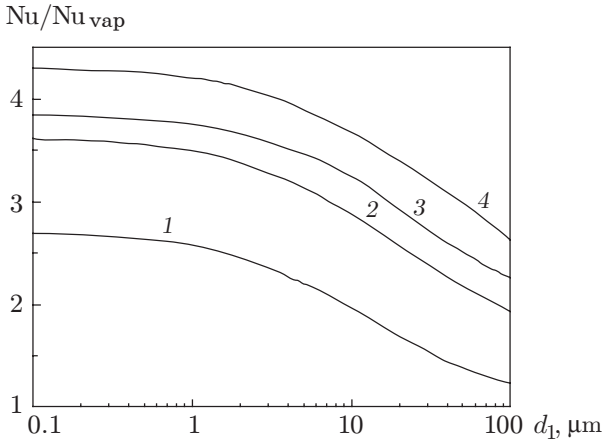

Fig. 5

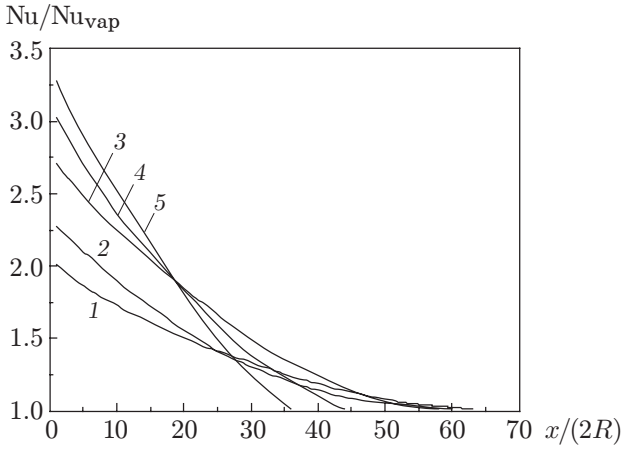

Fig. 6

Fig. 5. Heat-transfer intensification ratio $\mathrm{Nu}/\mathrm{Nu}_{\rm vap}$ versus inlet droplet diameter d_1 at $x/(2R) = 20$ and $\mathrm{Re} = 1.8 \cdot 10^3$ (1), 10^4 (2), $5 \cdot 10^4$ (3), and 10^5 (4).

Fig. 6. Heat-transfer intensification ratio versus air concentration for $\mathrm{Re} = 13{,}000$, $M_{\rm liq,1} = 0.1$, and $M_{\rm air,1} = 0$ (1), 0.01 (2), 0.1 (3), 0.2 (4), and 0.5 (5).

compared to that in a single-phase flow. An analysis of Fig. 4 allows the following conclusions to be made. The presence of evaporating droplets has an appreciable influence on heat-transfer intensification in the two-phase gas–vapor–droplet flow (the rate of heat transfer increases more than threefold), whereas the wall friction increases only insignificantly (roughly by 10%). An increase in the inlet droplet diameter increases the surface friction and decreases the heat-transfer intensity.

The impact of the inlet droplet diameter on the heat-transfer intensification ratio is illustrated by Fig. 5. An increase in the inlet droplet diameter (at a fixed mass concentration of the liquid phase) diminishes the intensity of heat- and mass-transfer processes; this effect can be attributed to the appreciable reduction of the interfacial contact area between the vapor–gas flow and the liquid droplets. For fine particles with $d_1 < 2$–5 μm, the ratio $\mathrm{Nu}/\mathrm{Nu}_{\rm vap}$ does not depend on the inlet droplet diameter. This range of particle sizes defines a steady-state evaporation regime with thermodynamic equilibrium between the vapor–gas mixture and the liquid phase. This conclusion is in line with the experimental data of [28].

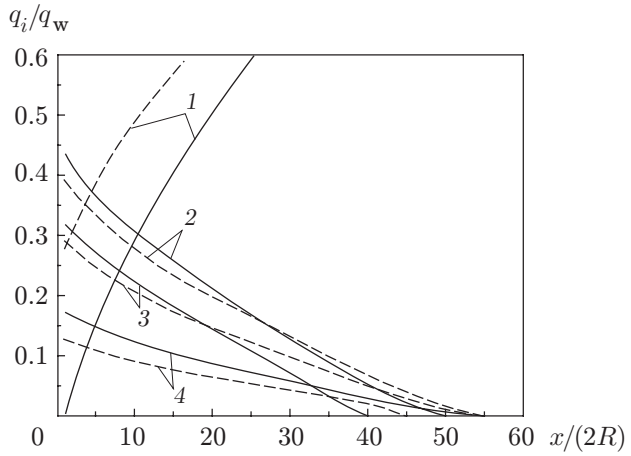

Fig. 7

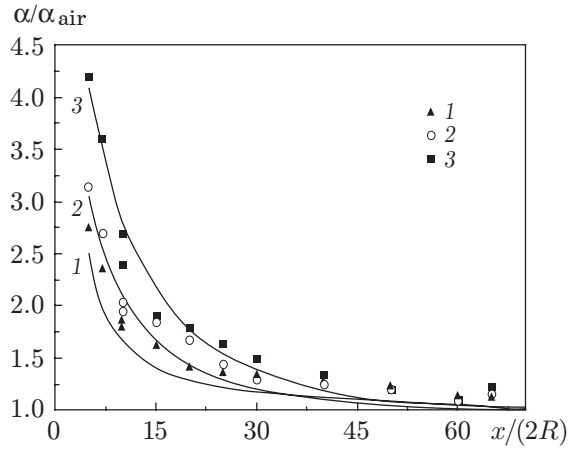

Fig. 8

Fig. 7. Distribution of individual components of the heat flux supplied to the duct surface in the two-phase gas–vapor–droplet flow with Re = 13,000 and $x/(2R) = 20$: q_{fl}/q_w (1), $q_{w,liq}/q_w$ (2), q_e/q_w (3), and q_{liq}/q_w (4); the solid and dashed curves refer to $M_{liq,1} = 0.1$ and $M_{liq,1} = 0.01$, respectively:.

Fig. 8. Comparison of the predicted data with the experimental data of [5]: $q_w = 14.53$ (1), 8.34 (2), and 6.4 kW/m^2 (3).

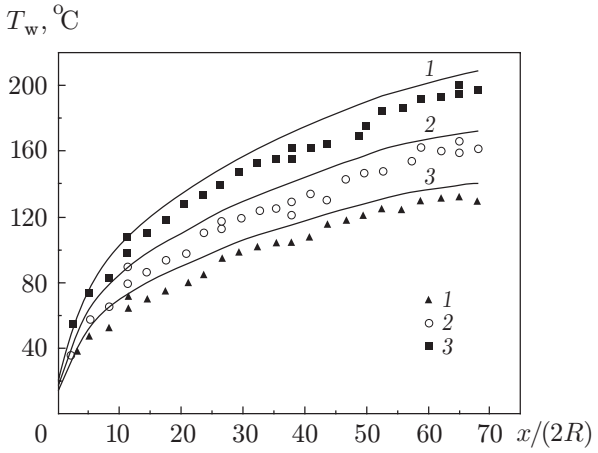

Fig. 9. Variation of wall temperature along the duct: the curves and the points refer to the computed data and experimental data of [6] for $q_w = 17.84$ (1), 13.92 (2), and 11.5 kW/m^2 (3).

The heat-transfer intensification ratio as a function of air concentration in the vapor–gas mixture is shown in Fig. 6. For the single-component vapor–droplet flow without air (curve 1), the ratio Nu/Nu_{vap} displays a minimum at $x/(2R) \lesssim 25$. With increasing air concentration, the heat-transfer rate increases since the diffusion of vapor from the droplet surface into the ambient flow becomes more intense; in this case, however, the length of the two-phase flow region in the downstream direction diminishes owing to the more intense droplet evaporation.

Such a complex multi-stage mechanism of heat transfer from the duct wall to the two-phase flow being operative, it is of interest to consider the contributions of various heat-flux components to the total heat flux on the wall. The distributions of individual heat-flux components over the duct length for various mass concentrations of the liquid phase are shown in Fig. 7 (q_{fl} is the heat flux spent on heating the vapor–gas flow, $q_{w,liq}$ is the conductive heat flux due to immediate wall-droplet contacts, q_e is the heat flux spent on droplet evaporation, and q_{liq} is the heat flux spent on droplet heating). From Fig. 7, the following conclusions can be drawn. In the inlet region of the heat-exchanging duct, a predominant portion of heat supplied to the duct wall is spent on conductive heat transfer and droplet evaporation. Further downstream, as the droplets undergo evaporation, the heat-flux components q_{liq}, $q_{w,liq}$, and q_e decrease, whereas the density of the heat flux to the vapor–gas phase permanently increases until the

ratio $q_{\text{fl}}/q_{\text{w}}$ finally reaches unity. In this case, a single-phase flow is established in the duct. A change in the inlet concentration of the liquid induces no fundamental changes in the proportion between various heat-flux components except for the initial region of the flow, where, at low concentrations $M_{\text{liq},1}$, the predominant part is played by the heat exchange with the vapor–gas mixture.

The heat-transfer intensification ratios for the wall-to-flow heat transfer in the gas–droplet flow, which were experimentally measured in [5] and predicted in the present work, are shown in Fig. 8 (α_{air} is the heat-transfer coefficient for the single-phase air flow under identical conditions). The input data for the computations were as follows: $M_{\text{liq},1} = 1.1$–2.1%, Re = 21,800–58,600, $2R = 12.95$ mm, computed length 0.889 m, $G_{\text{air}} = 4.02$–10.8 g/sec, $d_1 = 9$–23 μm, $\tau_+ = 139$–208, and $T_1 = 300$ K. The experiments were performed under atmospheric pressure. It is seen that, as the wall heat-flux density increases, the ratio $\alpha/\alpha_{\text{air}}$ monotonically decreases owing to the increase in wall temperature.

The measured distributions of the wall temperature T_{w} along the duct are shown in Fig. 9. The input data for the computations were chosen to reproduce the experimental conditions in [6]: $M_{\text{liq},1} = 0.5\%$, Re = 39,300, $2R = 13.2$ mm, computed length 0.924 m, $G_{\text{air}} = 7.58$ g/sec, $d_1 = 16$ μm, $\tau_+ = 272$, and $T_1 = 293$ K. The experiments were performed under atmospheric pressure. Figure 9 shows that the computed wall temperatures agree fairly well with the experimental data.

5. Conclusions. A physical model for heat and mass transfer in a turbulent gas–vapor–droplet flow in a cylindrical duct was developed. In this model, the liquid phase is a system of localized sinks of heat and localized sources of vapor. To calculate turbulent characteristics of the gas phase, we used the k–ε model of turbulence. A closed system of transfer equations was composed, which includes the continuity equation, equation of axial flow, the energy equation with a source term, the diffusion equation for the vapor–gas mixture with a source of vapor, and the heat- and mass-transfer equation for a single droplet. The model takes into account the deposition of droplets onto the duct wall and heat transfer due to immediate droplet–wall contacts.

A numerical heat- and mass-transfer study of a ducted turbulent two-phase gas–vapor–droplet flow was performed in which the thermal and gas-dynamic characteristics of the flow at the duct inlet were considered as variable parameters.

It is shown that, with increasing inlet droplet diameter, considerable intensification of heat transfer between the duct surface and the gas–vapor–droplet mixture occurs, whereas the increase in wall friction is insignificant.

With increasing mass concentration of liquid droplets, considerable intensification of heat- and mass-transfer processes is observed in the two-phase flow, with an increase in the fraction of heat spent on phase transition and heat transfer due to immediate droplet-wall contacts. The wall friction increases insignificantly.

An increase in the mass concentration of air considerably enhances the rate of heat transfer, simultaneously decreasing the length of the two-phase zone of the flow in the downstream direction. Good agreement between the computed values and available experimental data is obtained.

This work was supported by the Russian Foundation for Fundamental Research (Grants Nos. 01-02-16994 and 02-02-06327-mas).

REFERENCES

1. M. A. Styrikovich, V. S. Polonskii, and G. V. Tsiklauri, *Heat and Mass Transfer, and Hydrodynamics of Two-Phase Flows in Atomic Power Stations* [in Russian], Nauka, Moscow (1982).
2. V. I. Terekhov, M. A. Pakhomov, and A. V. Chichindaev, "Heat transfer in a tube laminar steam-drop flow," *Thermophys. Aeromech.*, **7**, No. 4, 499–511 (2000).
3. Y. Koizumi, T. Ueda, and H. Tanaka, "Post dryout heat transfer to R-113 upward flow in a vertical tube," *Int. J. Heat Mass Transfer*, **22**, 669–678 (1979).
4. A. G. Rane and S.-Ch. Yao, "Convective heat transfer to turbulent droplet flow in circular tubes," *Trans. ASME, J. of Heat Transfer*, **103**, No. 4, 679–684, (1981).
5. K. Mastanaiah and E. N. Ganic, "Heat transfer in two-component dispersed flow," *Trans. ASME, J. Heat Transfer*, **103**, No. 2, 300–306 (1981).
6. S. Sikalo, N. Delalic', and E. M. Ganic', "Hydrodynamics and heat transfer investigation of air–water dispersed flow", *Int. J. Exp. Thermal Fluid Sci.*, **25**, 511–521 (2002).
7. A. I. Leont'ev, "Extension of the limiting laws of friction and heat transfer to turbulent gas–liquid flows," *Izv. Sib. Otd. Akad. Nauk SSSR, Ser. Tekh. Nauk*, No. 10, Issue 7, 47–58 (1984).

8. V. I. Terekhov, M. A. Pakhomov, and A. V. Chichindaev, "Heat and mass transfer in a two-component developed turbulent gas–vapor–droplet flow," *Inzh.-Fiz. Zh.*, **74**, No. 2, 331–338 (2001).
9. V. I. Terekhov, M. A. Pakhomov, and A. V. Chichindaev, "Effect of evaporation of liquid droplets on the distribution of parameters in a two-species laminar flow," *J. Appl. Mech. Tech. Phys.*, **41**, No. 6, 1020–1028 (2000).
10. V. I. Terekhov and M. A. Pakhomov, "Numerical study of heat transfer in a laminar mist flow over an isothermal flat plate," *Int. J. Heat Mass Transfer*, **45**, 2077–2085 (2002).
11. R. G. Deissler, "Analysis of turbulent heat transfer, mass transfer, and friction in smooth tubes at high Prandtl and Schmidt numbers," Report No. No. 1210, NACA, Washington (1955).
12. Y. Nagano and M. Tagawa, "An improved k–ε model for boundary layer flow," *Trans. ASME, J. Fluid Eng.*, **109**, 33–39 (1990).
13. W. P. Jones and B. E. Lounder, "The calculation of low-Reynolds-number phenomena with a two-equation model of turbulence," *Int. J. Heat Mass Transfer*, **15**, 1119–1130 (1973).
14. H. K. Myong and N. Kasagi, "A new approach to the improvement of k–ε turbulence model for wall-bounded shear flows," *Int. J. JSME*, Ser. 2, **33**, 63–72 (1990).
15. S. S. Kutateladze and A. I. Leont'ev, *Heat and Mass Transfer and Friction in Turbulent Boundary Layer* [in Russian], *Énergoatomizdat*, Moscow (1985).
16. M. C. Yuen and L. W. Chen, "Heat transfer measurements of evaporating liquid droplets," *Int. J. Heat Mass Transfer*, **21**, 537–542 (1979).
17. I. N. Gusev, E. I. Guseva, and L. I. Zaichik, "Deposition of particles on channel walls in a turbulent flow," *Inzh.-Fiz. Zh.*, **59**, No. 5, 735–742 (1990).
18. H. Schlichting, *Boundary Layer Theory*, McGraw-Hill, New York (1979).
19. I. V. Derevich, "Statistical modeling of mass transfer in turbulent dispersed flow. 1. Model development," *Int. J. Heat Mass Transfer*, **43**, 3709–3723 (2000).
20. J. D. Anderson (Jr.), G Degrez, E. Dick, et al., *Introduction to Computational Fluid Dynamics*, J. F. Wendt (ed.), Springer Verlag, Berlin (1992).
21. J. G. M. Eggels, F. Unger, M. H. Weiss, et al., "Fully developed pipe flow: A comparison between direct numerical simulation and experiment," *J. Fluid Mech.*, **268**, 175–209 (1994).
22. J. Laufer, "The structure of turbulence in fully developed pipe flow," Report No. 1174, NACA Washington (1954).
23. A. Yu. Varaksin and A. F. Polyakov, "Experimental study of velocity fluctuations of bidispersed particles in turbulent air flow," in: *Gas-Dynamic and Heat- and Mass-Transfer Problems in Power Plants*, Proc. of the XII School–Seminar of Young Scientists and Specialists Headed by Academician A. I. Leont'ev (Moscow, May 25–28, 1999), MEI Publ. (1999), pp. 207–210.
24. T. J. Cramer and C. A. Depuw, "Experimentally determined mean flow characteristics of gas-solid suspension," *Trans. ASME, J. Fluids Eng.*, **94**, No. 2, 254–262. (1972).
25. A. A. Shraiber, L. B. Gavin, V. A. Naumov, et al., *Turbulent Gas-Suspension Flows* [in Russian], Naukova Dumka, Kiev (1987).
26. W. S. J. Uijetterwaal and R. V. A. Oliemans, "Particle dispersion and deposition in direct numerical and large eddy simulations of vertical pipe flow," *Phys. Fluids A*, **8**, 2590–2604 (1996).
27. A. Yu. Varaksin and A. F. Polyakov, "Experimental study of particle-velocity fluctuations in turbulent air flow," *Teplofiz. Vys. Temp.*, **38**, No. 5, 792–798 (2000).
28. A. V. Chichindaev, "Investigation of heat transfer to low-temperature water–aerosol flows," Ph. D. Thesis, Novosibirsk (1998).